



# Smart lost circulation materials for productive zones

Ahmed Mansour<sup>3</sup> · Arash Dahi Taleghani<sup>1</sup> · Saeed Salehi<sup>2</sup> · Guoqiang Li<sup>3</sup> · C. Ezeakacha<sup>2</sup>

Received: 20 September 2017 / Accepted: 3 April 2018 / Published online: 2 May 2018  
© The Author(s) 2018

## Abstract

Lost circulation has been a serious problem while drilling that may lead to heavy financial costs in the form of lost rig time and lost mud fluid. In severe cases, it can lead to well blowout with serious environmental hazards and safety consequences. Despite extensive advances in the last couple of decades, lost circulation materials used today still have disadvantages such as damaging production zones, failing to seal large fractures or plugging drilling tools. Here, we propose a new class of smart expandable lost circulation material (LCM) to remotely control the expanding force and functionality of the injected LCM. Our smart LCM is made out of shape memory polymers that become activated by formation's natural heat. Once activated, these particles can effectively seal fractures' width without damaging pores in the production zone or plugging drilling tools. The activation temperature of the proposed LCM can be adjusted based on the formation's temperature. We conducted a series of experiments to measure the sealing efficiency of these smart LCMs as a proof of concept study. Various slot disk sizes were used to mimic different size fractures in the formation. The API RP 13B-1 and 13B-2 have been followed as standard testing methods to evaluate this product.

**Keywords** Expandable lost circulation material · Static fluid loss · Dynamic fluid loss · Shape memory polymers

## List of symbols

$\emptyset_f$	Frozen portion of the SMP	$T_h$	Maximum temperature
$p_m$	Mud pressure	$V_{frz}$	Actual frozen volume
$p_p$	Pore pressure	$V$	Total volume
$T_0$	Initial temperature	$\epsilon_a^T$	Thermal strain in the active portion
$T_g$	Glass transitioning temperature	$\epsilon_a^e$	Entropic active strain
$\alpha$	Thermal expansion coefficient of SMP	$\epsilon_f^T$	Thermal Strain
$\alpha_a$	Thermal expansion coefficient of active portion of SMP	$\sigma_h$	Minimum horizontal stress
$\alpha_f$	Thermal expansion coefficient of frozen portion of SMP	$\sigma_H$	Maximum horizontal stress
$\alpha_T$	Thermal constant	$\sigma_T$	Thermal stress
$\epsilon_f^e$	Entropic frozen strain	$\sigma_{SMP}$	Total SMP stress release
$\epsilon_f^i$	Internal energetic strain	$\sigma_{Thermal}$	Thermal SMP stress release
$x$	A position vector	$\sigma_{\theta'}$	Effective hoop stress
$T_0$	Initial temperature	$\Delta T$	Change in temperature
$T$	Temperature	$\epsilon$	Total strain of the SMP
$\epsilon$	Total strain	$\theta$	Angle from the azimuth of the maximum horizontal stress
$\epsilon_s$	Strain from the free strain recovery test	$h$	Thickness of SMP
		$r_{SMP}$	Radius of SMP
		$E_i$	Young's modulus related to the internal energetic deformation
		$E_e$	Young's modulus related to the entropic deformation
		$\sigma_{eff}$	Effective relaxed stress
		$t$	Time
		$\tau_i$	Effective relaxation time
		$\epsilon_r$	Strain from free recovery

✉ Arash Dahi Taleghani  
arash.dahi@psu.edu

<sup>1</sup> Pennsylvania State University, State College, PA, USA

<sup>2</sup> Oklahoma University, Norman, OK, USA

<sup>3</sup> Louisiana State University, Baton Rouge, LA, USA

## Introduction

One of the most important decisions that need to be made in drilling operations is choosing the right type and density of drilling fluids. Drilling fluids are used in drilling operations to provide a pressure overbalance in the bottomhole and prevent the wellbore from collapsing. They are also used to cool down the drilling bits and transport cuttings to the surface. However, very often not all the drilling fluid is circulated back to the surface. Drilling fluid can be lost to the formation through fractures. Such incidents are called lost circulation events. Lost circulation is a costly problem due to creating non-productive time (NPT) while drilling, and if not controlled, it can cause serious environmental risks such as blowouts (Arshad et al. 2014). Table 1 shows the lower-end costs of lost circulation based on today's market prices. It can be seen that controlling a severe lost circulation incident can take from 3 to 7 days. It becomes more expensive if the lost circulation is on an offshore rig than on an onshore rig. It was seen that most lost circulation incidents occur in highly permeable, karsted or naturally fractured formations (Al-Saba et al. 2014a, b). Given that 26% of the wells around the world experience such problems, a solution to such problems would be very beneficial especially in low oil price time were marginal costs should be minimized by operators.

There are two general approaches to prevent or minimize lost circulation problems. The first approach is called the preventive approach. This method can be used when the drill engineer anticipates that a lost circulation event may occur in a specific zone, but has not yet occurred. In this approach, lost circulation can be prevented by adding materials to the mud that will seal fractures and strengthen the wellbore, therefore, preventing a fracture from further propagation or worsening the fluid loss. The second approach is called corrective lost circulation treatment and can be achieved by adding materials known as lost circulation materials. When mixed with the mud, lost circulation materials have the ability to plug the fracture and seal it if their particle size is big enough to do so. The type, shape, composition, size distribution and strength of the lost circulation materials (LCMs) can also be important to design an efficient solution treatment to address lost circulation (White 1956). In this paper,

**Table 1** Cost of lost circulation

	Onshore operation	Offshore operation
Number of days spent to control lost circulation	3	7
Cost per day of the drilling operation (\$)	65,000	120,000

we propose a smart expandable material made out of shape memory polymers that can seal the fracture and strengthen the wellbore.

Shape memory polymers have the ability to recover stress when inserted in a confined environment. The stress recovered is supposed to increase the circumferential compressional stress around the wellbore and may strengthen the wellbore by expanding the mud weight window.

To be able to understand how mud loss to the formation may occur during drilling and how to strengthen and stabilize the wellbore, we need to look at the stress distribution around the wellbore as drilling mud is primarily circulated in the bottomhole to keep the hole open and prevent the well from collapsing. Let's assume a vertical well, the effective hoop stress can be defined as

$$\sigma_{\theta r} = \sigma_H + \sigma_h - p_p - p_m - \sigma_T - 2(\sigma_H - \sigma_h) \cos 2\theta \quad (1)$$

By assuming that the tensile strength of rock is negligible, wellbore starts bleeding mud when hoop stress becomes tensile. The only parameter that the drilling engineer can control in the above equation is the mud weight ( $p_m$ ). Wellbore strengthening is achieved here by the compression induced by the expansion of LCM materials filling the fracture. Increasing the compressional hoop stress will prevent the fracture from propagating. Alberty and Mclean (2004) presented a stress cage model to explain that the hoop stress around the wellbore can be enhanced by sealing the fracture mouth (isolating them). Salehi (2012) tested the wellbore hoop stress enhancement theory using a 3D poro-elastic, finite element model and obtained the same results. Here, we extend strengthening process by actually increasing compressional hoop stress.

## Lost circulation materials

Wellbore instability has been estimated to cause economic losses of about 8 billion US dollars per year (Cook et al. 2012). From this 8 billion US dollars, it was estimated that lost circulation alone accounted for \$2–\$4 billion annual costs due to lost time (Cook et al. 2012). In the Gulf of Mexico, lost circulation, stuck pipe, sloughing shales and wellbore collapse account for 44% of the total non-productive time (Cook et al. 2012). The more non-productive time the well experiences will increase costs higher. Lost circulation does not only cause economic losses due to an increase in non-productive time. Uncontrolled loss of fluid can also damage the formation's productivity and lead to further economic losses. The use of synthetic-based muds that range from \$100 to \$200 per barrel makes losing these fluids extremely costly.

LCMs work in such a way that particles in the mud increase in size in order to plug the pores and cracks that mud alone cannot seal (White 1956). Materials should have certain characteristics to be used as a LCM, which are briefly discussed in API standards 13B-1 and 13B-2. For instance, if the size of the particles is too small for the given fracture width, the particles will flow through the fractures and particle bridging may never occur. Similarly, if the size of the particles is too big, the particles will not be able to enter the fracture, and therefore, sealing may not take place. Therefore, the size of the material particles and their distribution are very crucial for a fast and proper sealing of fractures. The materials should also be able to adapt to a wide range of environments, temperatures and pressures. The seal formed by the LCMs should be able to withstand mechanical forces that come from drilling mud, erosional forces that come from the moving particles in the mud as well as hydrodynamic forces that come from swab and surge (Cook et al. 2012). Lost circulation materials can be classified as fibrous, flaky, granular types or a mixture of the three types. The LCM can be effective if the bridge it forms inside the fracture can withstand all the forces mentioned earlier. In order to make sure that the LCM seals the fracture effectively, researchers have come up with theories to maximize the chance of bridging. Bridging of particles is defined as the buildup of solids that reduces inflow. Various jamming or bridging theories are available, and their main goal is to predict bridging time. Abrams (1977) proposed two rules to minimize formation damage due to lost circulation and mud invasion. The first rule suggests that the average particle size (D50) of the bridging materials or LCMs should be equal or slightly larger than a third of the average formation pore size. The second rule suggests that the LCM concentration should not be less than 5% by volume of the total solids in the mud formation. Whitfill (2008) proposed an alternative approach to optimize bridging considering fracture width instead of pore throat sizes. The average particle size of the LCM should be equal to the fracture width to make sure that the fracture is effectively plugged.

Despite continuous efforts to improve effectiveness of LCMs and understand the mechanisms involved in their placement, there are still some shortcomings. The biggest disadvantage LCMs face today is failure in sealing big fractures. According to Al-Saba et al. (2014a, b), these big fracture sizes have apertures that are equal to or larger than few millimeters wide, and LCMs fail to bridge properly to seal it. The second disadvantage is failure to work in high-pressure and high-temperature (HPHT) environments; the LCM seal is either not able to withstand the high pressures or it will melt due to high temperatures. Third, according to the private communications with field engineers, if LCMs are not soluble, they may damage production zones and therefore affect productivity, which could be a serious problem.

Finally, plugging drilling tools has been seen as an issue. LCMs that are too big in size sometimes may plug the tools and impose extra cost and service to control the well.

Looking at the disadvantages mentioned above, it is very clear that we need an LCM that can go through the drilling tools without plugging it and then through activation and expansion stage to plug big fractures and strengthen the wellbore.

## Shape memory polymers

The shape memory effect was first discovered by Chang and Read in 1932. Shape memory polymers (SMPs) are polymers that have the ability to be deformed and fixed into a temporary shape; they are then able to recover to their original permanent shape only when they are exposed to a specific external stimulus such as heat, light, magnetic field, moisture or pH. Not all polymers can be fixed in a temporary shape. For example, rubber can change shape whenever it's loaded, but when the load is removed the rubber goes back instantaneously to its original shape and no fixing of the temporary loaded shape has occurred. However, when the shape memory polymers are deformed when loaded, they have the ability to trap mechanical energy as internal energy and release this energy whenever an external stimulus causes a change in the molecular relaxation rate or in material morphology (Li 2014). Shape memory polymers not only have this shape-changing advantage but they are also cheap, lightweight, nontoxic, biocompatible and biodegradable (Ratna and Karger-Kocsis 2008).

The smart LCMs proposed in this paper will have temperature as an external stimulus. Shape memory polymers with temperature as an external stimulus can be either thermoset or thermoplastic. Thermoset SMPs are physically or chemically cross-linked polymers. They are usually preferred in engineering structures due to their high stiffness, high strength, high thermostability, high-dimensional stability and high corrosion resistance as compared to thermoplastic SMPs. During the shape recovery process, thermoplastic SMPs melt and, therefore, may not be an appropriate material to use as an LCM. The smart LCMs proposed here will have characteristics that stand between the thermoset and thermoplastic SMPs, a.k.a. ionic polymers or ionomers (Lu and Li 2016). Before explaining how smart LCMs will recover, seal fractures and strengthen the wellbore, there is a process called programming that needs to be done to achieve the mentioned advantages. Programming is the process that fixes the SMP in the temporary shape. A five-step thermomechanical cycle is used here for SMP programming as shown in Fig. 1.

This preparation process is called cold programming because the programming is conducted in the glassy state

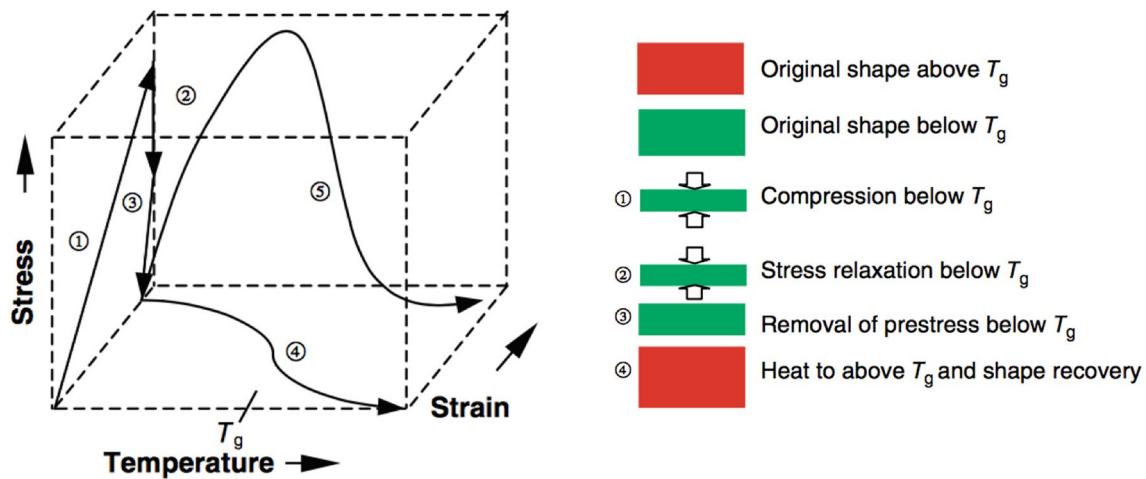


Fig. 1 Cold programming for thermoset SMPs (Li 2014)

(Li and Xu 2011; Li et al. 2013). From Fig. 1, the original shape of the SMP is prestressed and put under compression at a temperature below the glass transition temperature ( $T_g$ ) region. The glass transition temperature is the temperature at which the SMPs go from being in a hard and glassy state to a pliable state. The second step is called stress relaxation and it happens while keeping the strain constant but relaxing the stress. The third step is removing the load. This completes the programming. As for recovery, it has two representative modes. One is free shape recovery, as shown in the fourth step in Fig. 1. This happens whenever the SMP is heated to above  $T_g$ . It can also show stress recovery, as illustrated in step 5 in Fig. 1. Step 5 happens when the recovery is constrained and it is called constrained stress recovery.

It is noted that in programming of the shape memory polymers, the shape-changing properties allow the smart LCM to seal big fractures without plugging drilling tools or damaging production zones. Knowing the wellbore temperature profile, the smart LCM can be utilized in such a way that it will be small in size when entering the tool and then expand at a specific temperature within the fracture due to the difference between the mud and formation temperature. Therefore, the smart LCMs will have an advantage of sealing the fracture and preventing tool plugging. Because the smart LCM will also have stress recovery due to the constrained expansion, the wellbore can be strengthened by this stress release.

Siskind and Smith (2008) developed a model to predict the overall stress recovery of the activated SMP. Equation 2 shows the overall stress recovery from the SMP. The authors explain that the SMP has an initial volume and when this volume changes due to temperature, there will be a frozen volume portion ( $\varphi_f$ ) and an active volume portion ( $\varphi_a$ ). The active volume is the sum of the strain from the entropic and thermal components, while the frozen volume is the temporarily fixed

volume, which transfers to active volume during the recovery process. The strains from both components are then subtracted from the total strain ( $\epsilon$ ) of the SMP and multiplied by the Young's Modulus ( $E$ ) to calculate the overall stress recovery of the SMP. The total strain can be calculated using Eq. 3.

$$\sigma_{\text{overall}} = E \left( \epsilon - \int_0^{\varphi_f} \epsilon_f^e(x) d\varphi - \int_{T_0}^{T_g} [\varphi_f \alpha_f + (1 - \varphi_f) \alpha_a] dT \right) \quad (2)$$

$$\epsilon = \frac{1}{V} \int_0^{V_{\text{frz}}} \epsilon_f^e dV + [\varphi_f \epsilon_f^i + (1 - \varphi_f) \epsilon_a^e] + [\varphi_f \epsilon_f^T + (1 - \varphi_f) \epsilon_a^T] \quad (3)$$

Alternatively, Liu et al. (2006) proposed another model to calculate the overall stress recovery of the SMP:

$$\sigma_{\text{Overall}} = E \left( \epsilon - \epsilon_s - \int_{T_h}^T \alpha dT \right) \quad (4)$$

where  $E$  is given by

$$E = 1 / \left( \frac{\varphi_f}{E_i} + \frac{1 - \varphi_f}{E_e} \right) \quad (5)$$

$\varphi_f$  in the above equation is the volume fraction of the frozen phase, which is given as

$$\varphi_f = \frac{\epsilon_s}{\epsilon_{\text{pre}}} \quad (6)$$

According to Wang and Li (2015), the overall stress recovery can be divided into four components: relaxed

stress, thermal stress, memorized stress and residual programming stress. The relaxed stress occurs due to the SMP particles being constrained from expansion, and it reduces the overall stress recovery. The relaxed stress is given as

$$\sigma_{\text{Relaxed}} = \sigma_{\text{eff}} \left( 1 - \sum_{i=1}^n \exp \left( -\frac{t}{\tau_i} \right) \right). \quad (7)$$

The thermal stress occurs due to temperature rising. Since this is a constrained environment and free expansion is prohibited, stress is developed. Thermal stress can increase or decrease the overall stress based on the type of programming occurred. For example, it can be seen in Fig. 1 that the stress in step 5 will peak then decrease again; this peak is because of the thermal and entropic stresses. Subtracting the thermal stress will give a constant and more reliable stress release from the SMP. The thermal stress is calculated as

$$\sigma_{\text{Thermal}} = \int_{T_0}^{T_r} E(T) \alpha(T) dt \quad (8)$$

The memorized stress is the stress stored in the programming phase of the shape memory polymer. It is calculated by

$$\sigma_{\text{memorized}} = E(T) \cdot \varepsilon_r \cdot (1 - \varphi_f) \quad (9)$$

Finally, the residual programming stress is considered to be zero whenever there is an unloading phase in the programming of the SMP. The overall recovery stress in a confined environment is given by

$$\sigma_{\text{overall}} = \sigma_{\text{Thermal}} + \sigma_{\text{memorized}} + \sigma_{\text{residual}} - \sigma_{\text{relaxed}} \quad (10)$$

According to Li (2014), the relaxed stress was measured using an MTS Q-TEST 150 machine with a fully constrained recovery. Li and Xu (2011) tried to calculate the memorized stress by considering the stress relaxation effect during stress recovery. The memorized stress is the difference between the measured stress by the MTS machine and the thermal stress and stress relaxation. They used this basic relationship to calculate the relaxed stress. Figure 2 shows the relaxed stress of the pure SMP versus SMP-based syntactic foam (Li and Nettles 2010).

Both of these SMPs types were also prestressed with two different stress values. It can be seen that the more the SMP is prestressed, the higher the stabilized recovered stress. The recovery stress peaks first and then gradually reduces until stabilization, due to the combined effect of thermal stress, memorized stress release and stress relaxation at the higher recovery temperature. After 3-D confined compression programming, the SMP-based syntactic foam showed a recovery stress as high as 26 MPa (Li and Uppu 2010), meaning that it will cause compressional forces on the wellbore hoop stress. These compressional forces could help

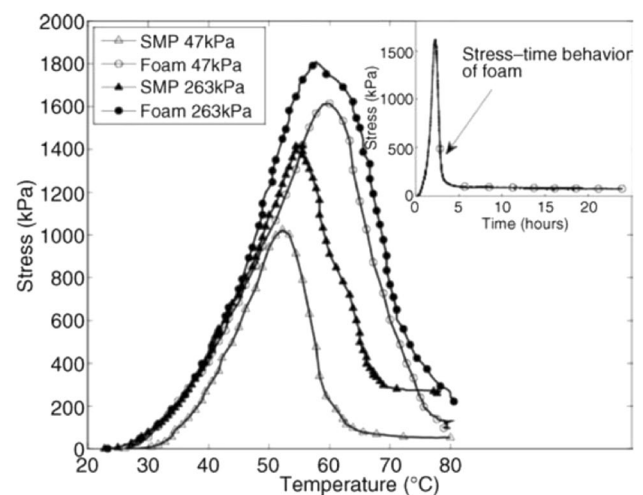


Fig. 2 Measured stress of different types of SMPs prestressed at different values (Li and Nettles 2010)

prevent the hoop stress from going into tension and could lead to wellbore strengthening. Finally, whenever a bundle of SMPs are present and are activated above  $T_g$ , their rubbery state allows them to bridge and connect together, forming an effective strong seal that isolates the fracture from the wellbore. When activated, the shape memory polymers use their ductility property to form bridges that are extremely hard to break. Therefore, there is a stress recovery advantage and a bridging advantage for LCMs made out of SMPs. It is also important to note that the smart LCMs will float in the mud due to their lower density. Adding surfactants to reduce the surface tension of the mud and disperse the particles will prevent such floating from occurring. SMPs have also been used as proppants (Santos et al. 2016) for re-fracturing operations (Santos et al. 2017) and in cementing applications (Taleghani et al. 2016).

## Static fluid loss experimental procedure

In this section, the smart LCM proposed in this paper was tested for its expansive and sealing properties using the particle plugging apparatus (PPA). The PPA is a high-pressure, high-temperature apparatus that can withstand up to 5000 psi and 500 °F. Four different types of tests conducted using this experiment are reported here. Preliminary results from Mansour et al. (2017a, b) are also presented in this paper.

The PPA consists of a hydraulic pump that pumps fluid and measures pressure to the nearest 100 psi, a PPA cell, a LCM receiver, a slot or tapered disk to represent the fracture in the formation, a thermostat to adjust the temperature, a thermometer that measures temperature to the nearest 1 °F and a measuring cylinder that measures fluid loss to the nearest 1 ml. A PPA cell schematic can be seen in Fig. 3.



The PPA cell is usually filled with a mixture of drilling fluid and LCMs. Then the slot disk is inserted on top of this mixture. The PPA cell has a floating piston in it which separates the oil coming from the hydraulic pump from the mixture of mud and LCM. The LCM receiver is then tightly capped at the top of the PPA cell and has a nozzle to allow the fluid that is lost from the PPA cell to be measured. The hydraulic pump is connected to the bottom of the PPA cell, where oil pushes the floating piston and if the slot or tapered disks are sufficiently sealed, then pressure builds up; if not, then fluid is lost and collected from the nozzle of the LCM receiver at the bottom of the apparatus.

The lost circulation material used in these experiments is made out of ionic shape memory polymers. The smart LCMs used here are manufactured in the form of disks, and their activation temperature is 158 °F and a melting temperature of 248 °F. As long as the temperature they are tested with is in between both temperatures, the particles will activate regardless of what the temperature is. The activation temperature is the temperature at which the smart LCM starts to expand and become a rubbery state. Disk-shaped particles settle down in the fractures along their thickness; hence,

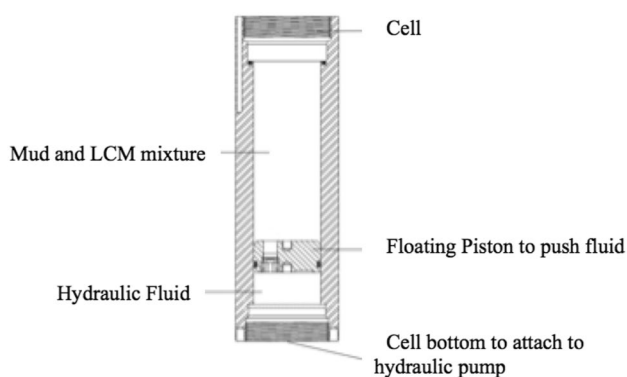


Fig. 3 Permeability plugging apparatus cell

their expansion will occur normal to the fracture plane which is required to get a better sealing and more stress release. Figure 4 shows the smart LCMs before and after activation.

The smart LCMs have a density of 59.3 lb/ft<sup>3</sup>, Poisson's ratio of 0.4, pre-strain (the maximum strain the LCM can achieve) of 25% and Young's modulus of 95,000, 37,710 and 350 psi at temperatures of −9.4, 73 and 176 °F, respectively. All experiments were done with the same type of smart LCMs but either shape or size was varied. The drilling fluid was made by adding 0.084 lb of bentonite to 0.092 gallons of water. The mud had a density of 8.9 ppg, and its formulation is provided in Table 2. 170 ml of this mud was taken, and the smart LCMs were added to this mud at a concentration of 0.3 lb of LCM per gallon of mud. This concentration of LCM is equivalent to almost 50 particles in the test sample. In one of the tests, the concentration was varied to see the relationship between smart LCM concentration and fracture sealing. The PPA cell is then filled with this mixture of drilling fluid and LCMs.

A mud rheogram was made by an Anton Paar modular compact rheometer to see the behavior of the mud (with no LCMs) with shear stress. The tests were conducted at 73 and 176 °F. Figure 5 shows the viscosity versus shear rate. Using Fig. 5, we can understand the apparent viscosity of the mud at room temperature and at the temperature from which the smart LCMs will activate. It can be seen that the higher the temperature the higher the apparent viscosity of the mud. This is also considered a shear thinning drilling fluid where the viscosity decreases with increasing shear rate.

Table 2 Mud formulation

Products	lb/gal (ppg)	% by weight	% by volume
Water	8.35	90.19	95.76
Bentonite	21.0	9.81	4.25

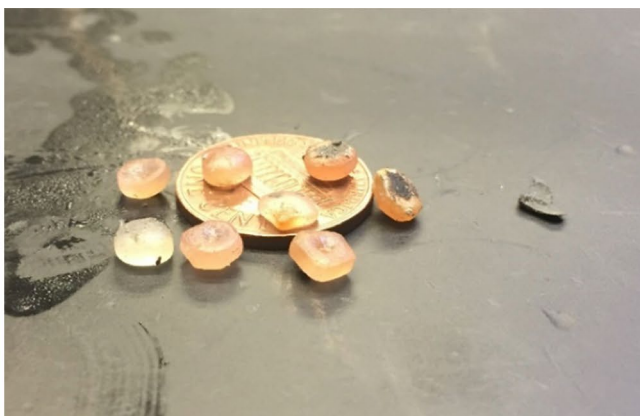
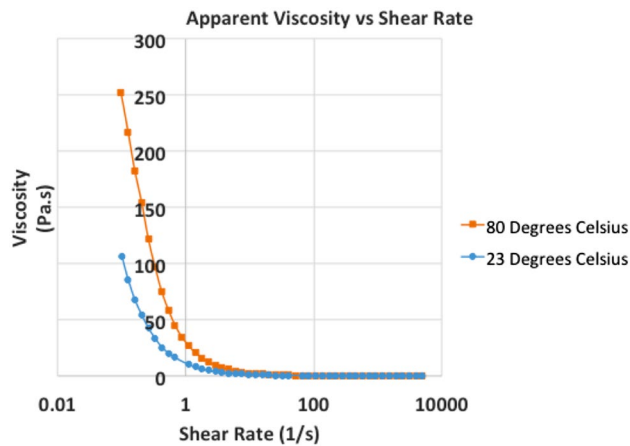


Fig. 4 Smart LCM before activation (left) and after activation (right)



**Fig. 5** Viscosity versus shear rate

**Table 3** Dimensions for disks

Type	Length (inches)	Width (inches)
Slot disk	0.279	0.1
Tapered disk	1.700	0.04–0.1

A slot disk or tapered disk is inserted on top of this mixture and on the top of the cell. The slot and tapered disk descriptions can be seen in Table 3. These dimensions are similar to the one used by Alsaba et al. to test the sealing of big fractures by conventional LCMs. Finally, all tests were repeated three times except the volumetric strain test which was repeated two times.

### Sealing efficiency test

The objective of this test is to check how effective the smart LCM is by measuring fluid loss and pressure buildup once the LCM is activated with respect to time. This experiment is supposed to show the decrease in fluid loss that the drilling engineer will see once the fracture is effectively sealed. The heating jacket was preheated to 167 °F. The LCMs used in this test were a mixture of two different diameter sizes. These sizes were 3 and 5 mm from which 0.15 ppg (lb/gal) of each smart LCM size was added to 170 ml of water-based mud and inserted in the PPA cell. The PPA cell was then inserted in the heating jacket and left there for 30 min before applying pressure, to allow the heat to be transferred to the cell to simulate downhole conditions. The fluid loss and the maximum pressure the seal can hold with respect to time were recorded. The fluid loss was measured by pumping hydraulic fluid in the cell at a rate of 2 ml/s. Since the fracture is being sealed with time, fluid is being prevented from going through the fracture and the pressure is building up. This pressure build up is also recorded with respect to time.

### Volumetric strain measurement test

The objective of this test is to analyze the volumetric change property of the LCM as a function of pressure. Since the wellbore is a partially constrained environment, the smart LCM will not be able to fully recover to its shape due to pressure from the bottomhole. Therefore, this experiment will help the drilling engineer understand how the smart LCMs will expand under various pressures. Two particles were picked, and their diameter, thickness and mass were measured. These two particles were then mixed with the water-based mud and put in the PPA cell. A disk with no fractures was used instead of a slot disk to allow the pressure to build up in the PPA Cell. Oil was pumped from the hydraulic pump to raise the pressure until 3000 psi, and then the temperature was raised to 176 °F and kept constant for 30 min. The pressure was then dropped gradually until it reached zero and the particles were then cooled down to room temperature, 73 °F. The particles were then taken out from the PPA cell, and their diameter, thickness and mass were measured. This experiment was repeated for pressures of 0, 1000 and 2000 psi.

### Permeability plugging test

The objective of this test is to measure the sealing efficiency of the smart LCM at 176 and 73 °F with respect to time and compare the results. This experiment will help drilling engineers understand the difference between the smart LCM and a normal LCM that has no expansive properties. It is also designed to see if the smart LCMs can still seal fractures if not activated.

### Concentration required for sealing test

The objective of this test is to experiment different concentrations of LCMs through the slot and tapered disk and see how much LCM is required to seal the fracture efficiently. The LCM particles used here had a shape of a thin sheet as opposed to disk shape in previous experiments. They were also much smaller in size ranging from 0.25 to 1 mm. They are made out of the same material but they have a different shape. So another objective of this experiment is to see if the shape of the material matters when trying to seal the fracture.

These smart LCMs were mixed with 170 ml of the drilling fluid at concentrations of 0.24, 0.48 and 0.96 lb/gal with the slot disk and the tapered disk. The heating jacket was set to a temperature of 185 °F, and the mixture was left there to settle for 30 min before running the test.

**Table 4** Design of experimental table

Mud blend	Temp. 1 (120 °F)	Temp. 1 (212 °F)
Base mud	Test 1	Test 4
Polymer blend	Test 2	Test 5
Polymer/fiber blend	Test 3	Test 6

**Table 5** Base mud formulation

Products	lb/bbl	% by weight	% by volume
Water	319.2	75.9	91.2
Gel	20.0	4.8	2.4
Caustic soda	0.5	0.1	0.1
Lignite	4.0	1.0	0.8
Desco	4.0	1.0	0.7
Barite	72.8	17.3	4.9

**Table 6** Smart LCM mud formulation

Products	lb/bbl	% by weight	% by volume
Water	313.0	74.4	89.4
Gel	20.0	4.8	2.4
Caustic soda	0.5	0.1	0.1
Lignite	4.0	1.0	0.8
Desco	4.0	1.0	0.7
Polymer LCM	5.0	1.2	1.7
Barite	74.0	17.6	4.9

## Dynamic fluid loss experimental procedure

The objective of the dynamic fluid loss experiments conducted in this study is to quantify the fracture-sealing efficiency of the smart LCM. Table 4 shows the experimental design where the mud blend and temperature are two independent variables. The dependent variable is the cumulative mud loss. Water-based mud (WBM) was used as the control base fluid. Table 5 shows that the control base fluid was formulated with mud additives that would have little to no impact on the fluid loss and filtration property. 5 lb/bbl of the swellable polymer LCM was used in formulating the second recipe as shown in Tables 6 and 7. Based on the fluid loss test results from the second recipe and some preliminary tests, a combination of the smart LCM and fiber LCM, 5 lb/bbl each, was used in formulating the third recipe. 120 and 212 °F were chosen as the low and high temperature levels, respectively, and 10 ppg was selected as the design mud weight.

According to Ghalambor et al. (2014), lost circulation and drilling fluids invasion are classified into losses

**Table 7** Smart/fiber LCM mud formulation

Products	lb/bbl	% by weight	% by volume
Water	310.0	73.7	88.6
Gel	20.0	4.8	2.4
Caustic soda	0.5	0.1	0.1
Lignite	4.0	1.0	0.8
Desco	4.0	1.0	0.7
Polymer LCM	5.0	1.2	1.7
Fiber	5.0	1.2	1.0
Barite	72.0	17.1	4.8

through pore throats, losses through induced and natural fractures and losses through vugs and carvens. In this study, a 2000- $\mu\text{m}$ -width fracture cylindrical slot was used because this fracture size falls within the range of typical induced fracture widths observed from Petrophysics image logs. In addition, Alsaba (2015) performed similar static condition tests using this fracture size. Figure 6 (left) shows two parts (top and bottom) of the cylindrical core slot. The bottom part shows the fracture orientation and a fracture length of 10,000  $\mu\text{m}$ . The dimensions of the entire cylindrical slot are: O.D = 1.5 inches, I.D = 1.0 inches and length = 1.1 inches. Figure 6 (right) shows that the core slot is carefully secured inside a core holder such that the only fluid exit from the entire system would be through the fracture.

Furthermore, most of the experiments that have been used to quantify fracture-sealing efficiency of LCM drilling fluids have been conducted in static conductions (Alsaba 2015; Guo et al. 2014; Kumar and Savari 2011; Hettema et al. 2007; Aston et al. 2004). In real-time drilling, bottomhole conditions are often in a dynamic mode, and a greater percentage of drilling fluids invasion occur during this time because the inertia state of the mud is surpassed by the hydrodynamic condition of mud particles and the fluids shearing action (Ezeakacha et al. 2016). Figure 7 shows the various stages of setting up the machine used in characterizing dynamic drilling fluid loss, for wellbore-shaped core samples and slots. The experimental procedure was programmed to track real-time data every 5 s, and operating parameters include but not limited to fluid loss through the fracture, rotary speed, temperatures (bath and sample) and pressures (back and cell). Based on previous tests and preliminary calibrations, 50 RPM, 100 psi and 200 psi were chosen as the rotary speed, back pressure and cell pressure, respectively.





**Fig. 6** 2000- $\mu\text{m}$ -width fracture slot (left) and well-secured fracture slot in a core holder (right)



**Fig. 7** Core holder with slot placed inside a mud cylindrical holder (left). Rotating shaft, temperature sensor and heating bath (middle). Complete setup of the dynamic mud loss experiment (right)

## Static fluid loss results and discussions

As mentioned above, four tests were made using the static fluid apparatus to test the smart LCMs. In this section results obtained for each test will be explained.

## Sealing efficiency test

The objective of this test is to see how effective the smart LCM is and measure fluid loss and pressure buildup once the LCM is activated with respect to time. Figure 8 shows

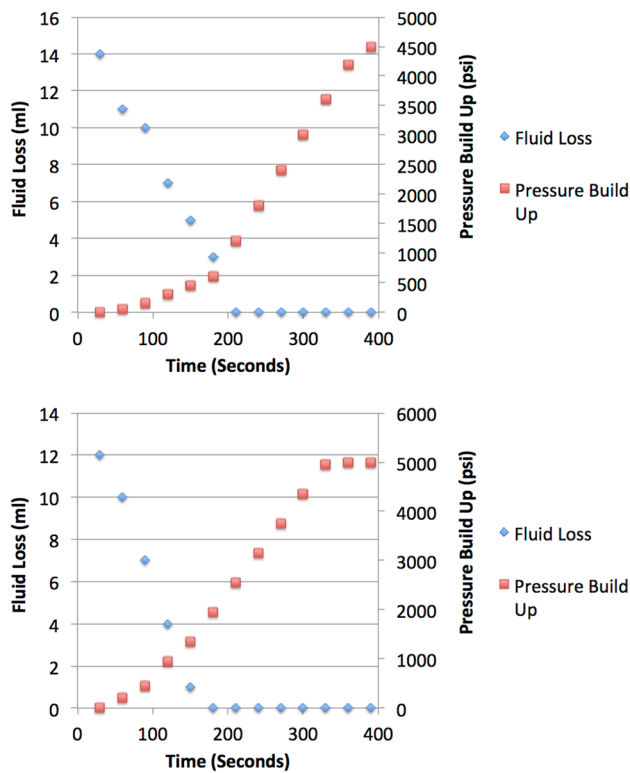


Fig. 8 Results for slot disk (top) and tapered disk (bottom)

the results that were obtained for the slot disk and the tapered disk.

It can be seen from the results that the fluid loss decreased gradually to zero as the particles expanded and started bridging. The particles are able to form cohesive bridges with each other once activated as seen in Fig. 9.

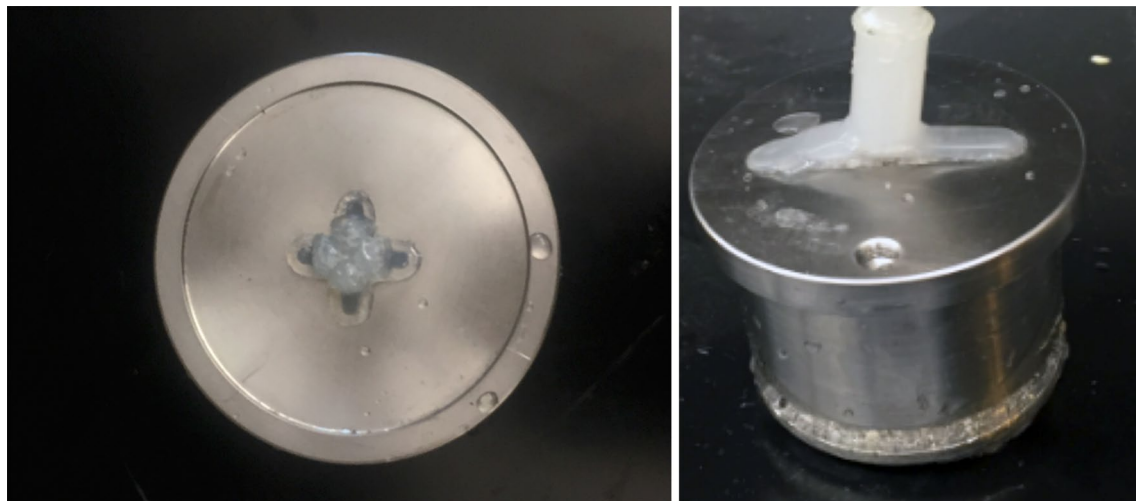


Fig. 9 Sealed slot disk (left) and sealed tapered disk (right)

These bridges are so hard to break that they are able to withstand pressures up to 5000 psi.

### Volumetric strain measurement test

The objective of this test is to analyze the volumetric change property of the LCM as a function of pressure. It was seen that there was no change in mass. Table 8 shows the measurements and volumetric expansion for each pressure.

The change in volume ( $dv/v$ ) was calculated by its variation with respect to changes in its radius and thickness

$$\left(\frac{dv}{v}\right)_{SMP} = 2\frac{\delta r}{r} + \frac{\delta h}{h} \quad (11)$$

The average  $dv/v$  was then plotted versus the surrounding hydrostatic fluid pressure as seen in Fig. 10. It can be seen that the higher the pressure is, the harder it is for the SMP to expand and recover its original shape. It also means that the less the expansion the smart LCM shows the higher the recovered stress that will act as compressional forces on the wellbore. Drawing a line of best fit, a linear correlation can be calculated for such behavior. At atmospheric conditions, maximum recovery occurs.

### Permeability plugging test

The objective of this experiment is to compare the sealing efficiency of an activated smart LCM with a non-activated smart LCM. Table 9 shows the test parameters.

The smart LCMs had an average diameter volume of size of  $30.06 \text{ mm}^3$ . The LCMs were added to 170 ml of mud at a concentration of 0.3 ppg. The mixture was then placed in the PPA cell. A slot disk was used to represent the fracture in the formation and placed on top of the PPA cell.

**Table 8** Results for volumetric strain measurement test

	0 psi	1000 psi	2000 psi	3000 psi
<b>First test</b>				
Initial diameter (mm)	5.05	5.21	6.14	4.29
Thickness (mm)	1.82	1.96	2.02	1.81
Diameter after expansion (mm)	4.82	4.97	5.49	4.2
Thickness after expansion (mm)	3.36	3.33	2.84	1.95
dv/v	0.755	0.607	0.194	0.0354
<b>Second test</b>				
Initial diameter (mm)	5.55	4.91	5.07	5.5
Thickness (mm)	2.39	1.79	2.03	2.01
Diameter after expansion (mm)	5.23	4.17	4.67	5.47
Thickness after expansion (mm)	4.65	3.21	2.69	2.07
dv/v	0.830	0.492	0.167	0.019
Average dv/v for both tests				
Average dv/v	0.79	0.55	0.18	0.03

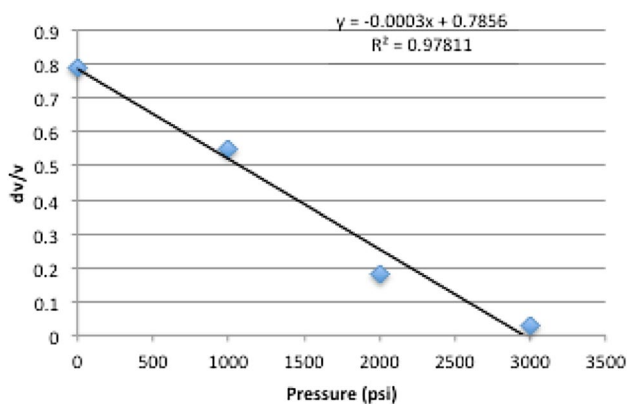


**Fig. 10** Change in volume of smart LCM versus pressure

**Table 9** Test parameters for permeability plugging test

	Test 1 @176 °F	Test 2 @73 °F	Test 3 @73 °F
Average particle volume (mm <sup>3</sup> )	30.06	30.06	32.20

The LCM receiver was then tightly capped onto the PPA cell, and the hydraulic pump was attached. The thermostat was then adjusted to 176 °F, and the mixture was left to settle at this temperature for 8 min. After that, oil was pumped from the hydraulic pump at a rate of 2 ml/s. Every 30 s, the fluid loss and the pressure that the seal can hold were recorded as seen in Fig. 11. The pressure reached to 3000 psi and was not allowed to exceed it.

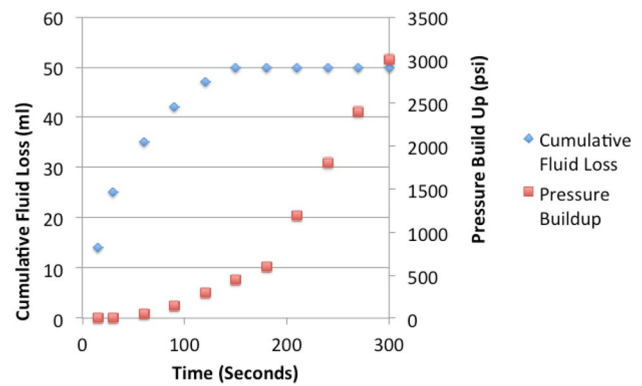


**Fig. 11** Fluid loss and pressure buildup at 80 °C

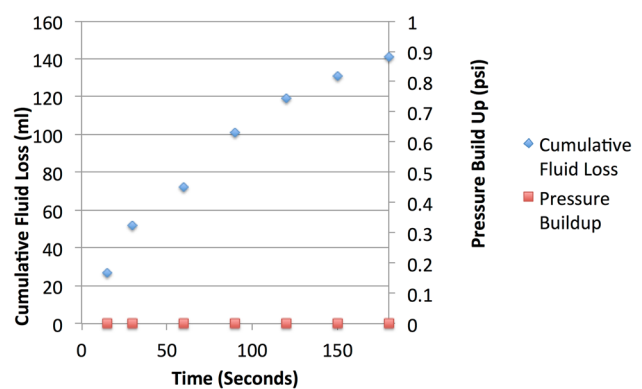


**Fig. 12** Results for normal size non-activated LCM at 23 °C

From Fig. 10, it is known that the particles expand by about 3% when under 3000 psi pressure. Therefore, to understand if these particles can plug the fracture way below activation temperature (73 °F) two extra experiments were made. For test 2, the objective was to see if the particles at a non-expanded size could seal the fracture alone without getting activated. Therefore, the particle volume used was the same as the one used in test 1 which is 30.06 mm<sup>3</sup>. For test 3, assuming that the only reason the smart LCMs sealed the particles was because they expanded in size, the LCMs used here has a bigger size where the particles had an average volume of 32.2 mm<sup>3</sup> at room temperature and they were tested to see if they could plug the fracture. Figures 12 and 13 show the results of these two tests.

It can be seen from the results above that it is the expansive property that the LCM has that allows it to seal the fracture. What makes the smart LCM an excellent choice for sealing fractures is that it has the ability to take the shape of the fracture by bridging and sticking together and at the same time still being able to withstand very high pressures.

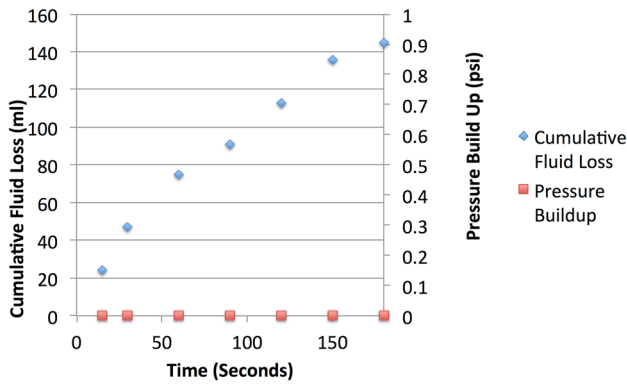


Fig. 13 Results for expanded size non-activated LCM at 23 °C

**Concentration required for sealing test**

The objective of this test is to experiment different concentrations of LCMs through the slot and tapered disk and see how much LCM is required to seal the fracture efficiently. Figure 14a, b shows the fluid loss and pressure buildup versus time for the slot disk at each concentration, respectively. It can be seen that as the concentration increases fluid loss does decrease but not by a large amount. The pressure that the

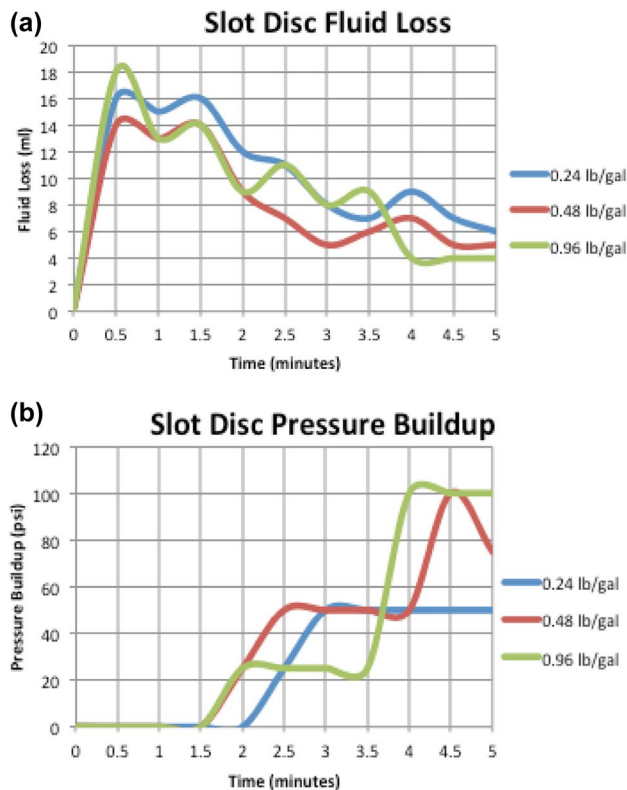


Fig. 14 a Fluid loss versus time for slot disk. b Pressure buildup versus time for slot disk

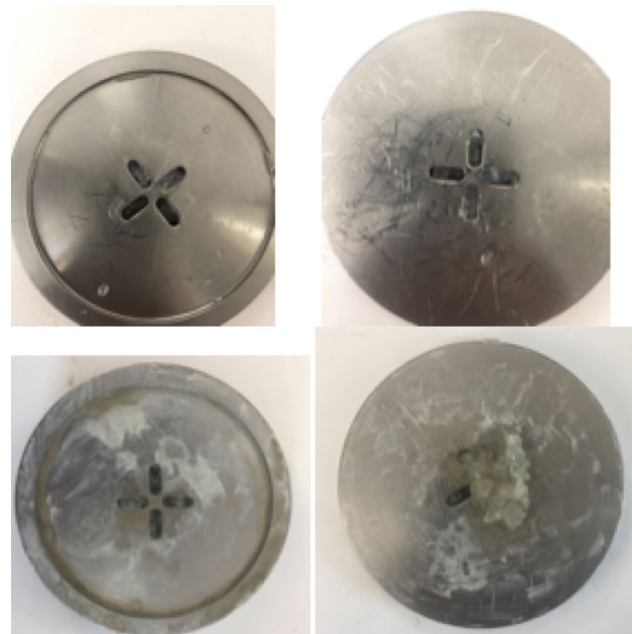


Fig. 15 Slot disk sealed with 0.24 lb/gal of LCMs (top row) versus 0.48 lb/gal (bottom row)

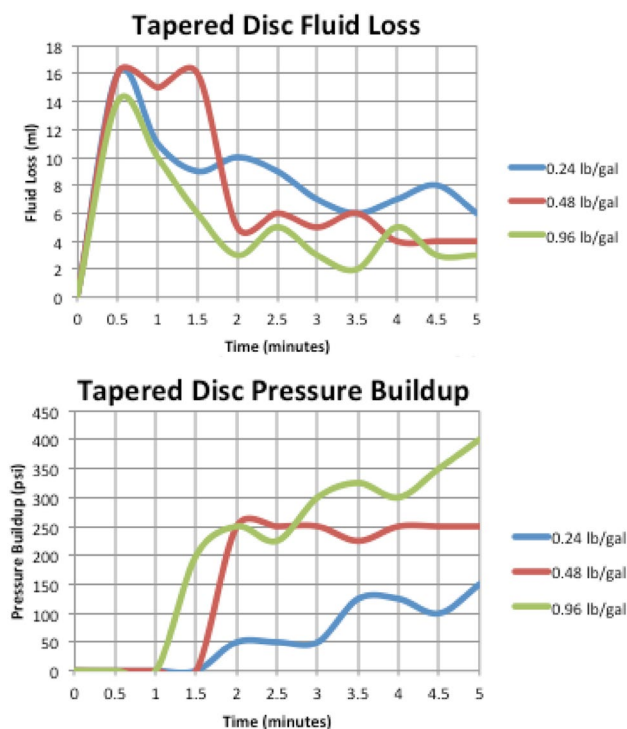
seal can hold was not also very high as opposed to previous experiments.

Figure 15 shows the slot disk sealed at two different concentrations. It can be seen that as the concentration increases, particles start to buildup beneath the actual fracture and form bridges with each other.

Figure 16 shows the fluid loss and pressure buildup versus time for the tapered disk at each concentration, respectively. It can be seen that fluid loss also decreases with increasing concentration and the pressure that the seal can hold increases with increasing concentration. However, the particles here caused a much higher pressure buildup than that in the slot disk. The particles tend to cause lower fluid losses and higher pressure buildups when the fracture is long in length as opposed to short in length.

The concentration of the LCMs therefore has an effect on how effectively the smart LCMs can seal. The bridges that this shape formed were not as strong as the bridges that the disk shapes formed. Even though the pressure buildups were not as high as the previous experiments that used, 3 lb/gal for concentration of LCMs, they still show a decrease in fluid loss and were able to withstand a reasonable differential pressure that will be seen in the wellbore whenever it is in an overbalance state.





**Fig. 16** Fluid loss for tapered disk (top) and Pressure buildup for tapered disk (bottom)

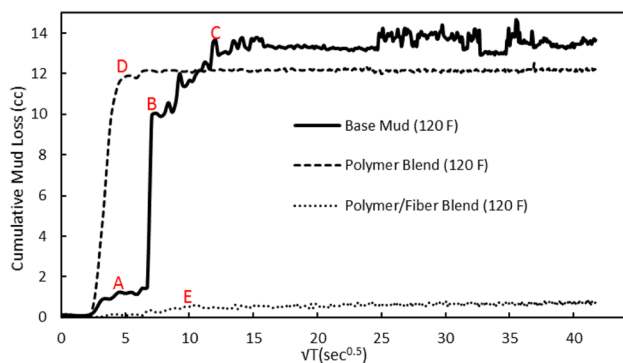


**Fig. 17** Dynamic drilling fluid loss pattern at 120 °F with different mud formulations

## Dynamic fluid loss experiment: procedure and results

The results from the dynamic fluid loss experiments are presented in Figs. 17, 18, 19 and 20. The alphabetical nomenclatures are used to denote points of interest during data acquisition and analyses. Figure 17 shows the mud loss patterns at 120 °F. For the base mud, the first significant loss was recorded as 1.448 cc, after 40 s and at 40 psi differential pressure. Point B showed the most significant loss of 10.052 cc after 65 s at 49 psi differential

pressure. The gradual increase from point B to C indicates the formation of filter cake within the fracture. After 3 min and 15 s, 13.672 cc was collected at 103 psi differential pressure. This was the cumulative loss for this experiment. With the swellable polymer LCM mud, the first and only notable loss occurred between 10 and 20 s. Point D shows that at 20 s, 11.469 cc was collected at 18 psi differential pressure. Further increase in pressure showed very minimal loss because the cumulative loss at the end of the experiment was 12.203 cc. In addition, the 100 psi differential pressure target was achieved after 3 min. Although the difference in final volumes of the base mud and swellable polymer blend is 1.496 cc, the plots reveal that the polymer blend exhibited better filter cake quality and stability after its loss through the fracture. A combination of fiber with the polymer blend resulted in better sealing efficiency. Stable filter cake was formed within the fracture, and this is evident from the steady but minimal increase in filtrate loss from point E onwards. The cumulative filtrate loss using this optimum LCM recipe (swellable polymer/fiber blend) at 120 °F was 0.818 cc. In a similar study involving vertical fracture creation and seal at 120 °F, Ezeakacha et al. (2017a, b) recorded 26.7% decrease in cumulative filtrate loss using a wellbore strengthening material recipe. Figure 18 shows the O.D and I.D of the bottom part of the fracture core slot, after the polymer/fiber blend experiment. The LCM particles can be seen within the fracture, and a fiber particle can be visually observed toward the right side of the I.D, very close to the fracture opening.

Figure 19 shows the mud loss patterns at 212 °F. Five notable points were observed for the base mud experiment. The first significant loss occurred from 5 to 15 s. At point A (15 s), 9.79 cc was collected at 21 psi differential pressure. There were signs of gradual filter cake evolution for the next 30 s, but an increase in differential pressure up to 53 psi damaged the thin filter cake and reopened the fracture. This resulted in 24.795 cc after 1 min at point B. Cook et al. (2016) commented on a similar observation. They studied the mechanical performance of a thick and thin external filter cake, on a narrow and wide fracture opening, respectively. The result of their study revealed that a thin filter cake would move more rapidly into the fracture than the thick filter, in response to differential pressure increase. Points C, D and E are responses to an increase in differential pressure for 62, 78 and 90 psi, respectively. A total of 35.052 cc was collected.

In the swellable polymer mud experiment, the first notable loss occurred at 25 s. Point F shows that at 25 s, 7.534 cc was collected at 9 psi differential pressure. The next 1 min revealed filter cake build up until a 55 psi differential pressure surged the mud loss to 13.777 cc at point G. From this point onwards, increase in pressure resulted in minimal filtrate loss, and the cumulative loss was recorded as 15.456 cc.



Fig. 18 Plugged fracture core slot after the polymer/fiber blend dynamic fluid loss test at 120 °F

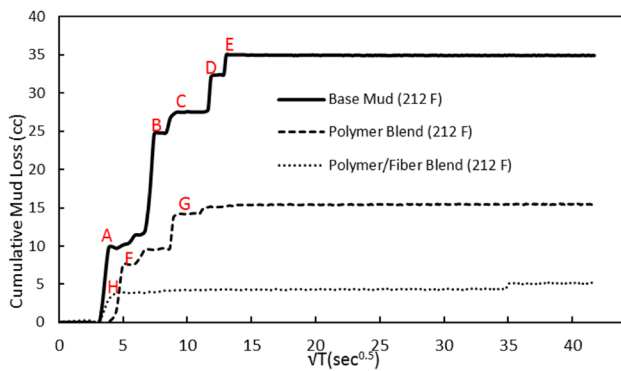


Fig. 19 Dynamic drilling fluid loss pattern at 212 °F, with different mud formulations

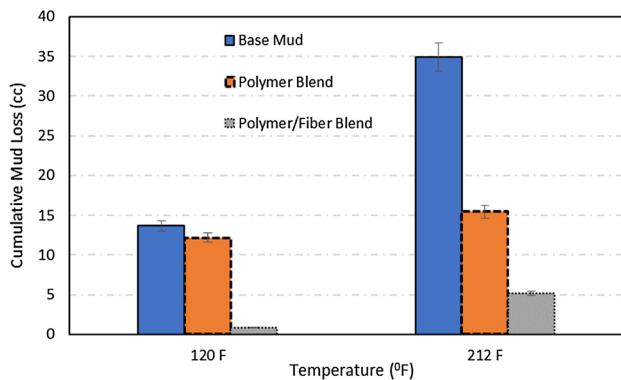


Fig. 20 Comparison of cumulative dynamic drilling fluid losses

Similar to the experiment at 120 °F, a combination of fiber with the swellable polymer blend resulted in better sealing efficiency at 212 °F. A stable filter cake was formed within the fracture at point *H*, and this is evident from the steady but very minimal increase in filtrate loss from this point onwards. 5.173 cc was the cumulative filtrate loss from the polymer/fiber LCM recipe at 212 °F. In the O.D and I.D of the bottom part of the fracture core slot from the polymer/fiber mud experiment, the LCM particles could be visually observed to have plugged the fracture completely, thus reducing the amount of fluid loss at the operating conditions. Figure 20 shows the comparison of all the cumulative loss data. The polymer blend has been reported to swell and expand at temperatures above 172 °F, suggesting its high performance in reducing fluid loss at 212 °F.

### Conclusion

A new type of smart expandable lost circulation material is introduced in this paper to reduce and prevent fluid loss and strengthen the wellbore. The smart expandable LCM was tested experimentally via static fluid loss and dynamic fluid loss apparatus to evaluate the LCM’s sealing efficiency. Some of the specific conclusions can be:

- The expansive properties of the proposed LCM make it an effective solution to bridging and sealing of vugs and fractures.

- According to static fluid loss tests, the smart LCM's seal can withstand up to 5000 psi differential pressure without breaking.
- The smart LCM is highly dependent on temperature and if not activated will not prevent fluid loss.
- The smart LCM induces compressive stress to strengthen the wellbore without damaging the reservoir permeability.
- Dynamic fluid loss tests indicate that the smart LCMs work more effective when combined with fibers.
- These materials can be comparatively cost effective for operators if used as preventive measure to reduce total non-productive time associated with corrective measures.

**Acknowledgements** The author would like to thank LSU Foundation for supporting development of this technology under LIFT2 program. Second author would like to thank Grace Instrument for letting us to conduct experiments on M2200 equipment. Special thanks go to Mr. Frank Bi in Grace Instrument and Mr. Jizhou Fan at LSU for compression programming the ionomers.

**Open Access** This article is distributed under the terms of the Creative Commons Attribution 4.0 International License (<http://creativecommons.org/licenses/by/4.0/>), which permits unrestricted use, distribution, and reproduction in any medium, provided you give appropriate credit to the original author(s) and the source, provide a link to the Creative Commons license, and indicate if changes were made.

## References

- Abrams A (1977) Mud design to minimize rock impairment due to particle invasion. *J Petrol Technol* 29(05):586–592
- Alberty MW, McLean MR (2004) A physical model for stress cages. Paper SPE 90493, presented in SPE annual technical conference and exhibition, Houston, USA
- Alsaba MT (2015) Investigation of lost circulation materials impact on fracture gradient. PhD dissertation, Missouri University of Science and Technology
- Al-Saba MT, Nygaard R, Saasen A, Nes OM (2014) Laboratory evaluation of sealing wide fractures using conventional lost circulation materials. Paper SPE 170576, presented in SPE annual technical conference and exhibition. Society of Petroleum Engineers, Amsterdam, The Netherlands
- Al-Saba MT, Nygaard R, Saasen A, Nes OM (2014) Lost circulation materials capability of sealing wide fractures. Paper SPE 170285, presented in SPE deepwater drilling and completions conference. Society of Petroleum Engineers, Galveston, TX, USA
- Arshad U, Jain B, Pardawalla H, Gupta N, Meyer A (2014) Engineered fiber-based loss circulation control pills to successfully combat severe loss circulation challenges during drilling and casing cementing in northern Pakistan. Paper SPE 169343, presented at the SPE Latin American and Caribbean petroleum engineering conference. Society of Petroleum Engineers, Maracaibo, Venezuela
- Aston MS, Alberty MW, McLean MR, Jong H, Armagost K (2004) Drilling fluids for wellbore strengthening. Paper-SPE-87130-MS, presented in IADC/SPE Drilling Conference, Dallas, TX, USA
- Cook J, Growcock F, Guo Q, Hodder M, van Oort E (2012) Stabilizing the wellbore to prevent lost circulation. *Oilfield Rev* 23(4):26–35
- Cook J, Guo Q, Way P, Bailey L, Friedheim J (2016) The role of filtercake in wellbore strengthening. Paper IADC/SPE 17899-MS, presented in IADC/SPE drilling conference and exhibition, Fort Worth, TX, USA
- Ezeakacha C, Salehi S, Ghalambor A, Karimi (2016) An integrated study of mud plastering effects for reducing filtrate's invasion. <https://doi.org/10.2118/179016-MS>.
- Ezeakacha CP, Salehi S, Bi H (2017) How does rock type and lithology affect drilling fluids filtration and plastering. Paper AADE-NTCE-094, presented in AADE national technical conference and exhibition, Houston, TX, USA
- Ezeakacha CP, Salehi S, Hayatdavoudi A (2017b) Experimental study of drilling fluid's filtration and mud cake evolution in sandstone formations. *ASME. J Energy Resour Technol* 139(2):022912
- Ghalambor A, Salehi S, Shahri M, Karimi M (2014) Integrated workflow for loss circulation prediction. Paper-SPE 168123-MS, presented in SPE international symposium and exhibition for formation damage and control, Lafayette, LA, USA
- Guo Q, Cook J, Way P, Ji L, Friedheim JE (2014) A comprehensive experimental study on wellbore strengthening. Paper IADC/SPE 167957-MS, presented in IADC/SPE drilling conference and exhibition, Fort Worth, TX, 4–6 Mar 2014
- Hettema M, Horsrud P, Taugbol K, Friedheim J, Huynh H, Sanders MW, Young S (2007) Development of an innovative high-pressure testing device for the evaluation of drilling fluid systems and drilling fluid additives within fractured permeable zones. Paper OMC-2007-082, presented in Offshore Mediterranean Conference and Exhibition, Ravenna, Italy
- Kumar A, Savari S (2011) Lost circulation control and wellbore strengthening: looking beyond particle size distribution. Paper AADE-11-NTCE-21, presented in AADE national technical conference and exhibition, Houston, TX, USA
- Li G (2014) Self-healing composites: shape memory polymer based structures. Wiley, West Sussex
- Li G, Nettles D (2010) Thermomechanical characterization of a shape memory polymer based self-repairing syntactic foam. *Polymer* 51(3):755–762
- Li G, Uppu N (2010) Shape memory polymer based self-healing syntactic foam: 3-D confined thermomechanical characterization. *Compos Sci Technol* 70(9):1419–1427
- Li G, Xu W (2011) Thermomechanical behavior of thermoset shape memory polymer programmed by cold-compression: testing and constitutive modeling. *J Mech Phys Solids* 59(6):1231–1250
- Li G, Ajisafe O, Meng M (2013) Effect of strain hardening of shape memory polymer fibers on healing efficiency of thermosetting polymer composites. *Polymer* 54(2):920–928
- Liu Y, Gall K, Dunn ML, Greenberg AR, Diani J (2006) Thermo-mechanics of shape memory polymers: uniaxial experiments and constitutive modeling. *Int J Plast* 22:279–313
- Lu L, Li G (2016) One-way multi-shape memory effect and tunable two-way shape memory effect of ionomer poly(ethylene-co-methacrylic acid). *ACS Appl Mater Interface* 8(23):14812–14823
- Mansour AK, Taleghani AD, Li G (2017) Smart expandable LCMs; a theoretical and experimental study. Paper AADE-17-NTCE-074, presented at the 2017 AADE national technical conference and exhibition in Houston, TX, USA
- Mansour AK, Taleghani AD, Li G (2017) Smart lost circulation materials for wellbore strengthening. Paper ARMA 17-0492, presented at the 51st US rock mechanics/geomechanics symposium in San Francisco, CA, USA
- Ratna D, Karger-Kocsis J (2008) Recent advances in shape memory polymers and composites: a review. *J Mater Sci* 43:254–269
- Salehi S (2012) Numerical simulations of fracture propagation and sealing: implication for wellbore strengthening. PhD dissertation,

- Department of Geological Sciences and Engineering, Missouri University of Science and Technology, USA
- Santos L, Dahi Taleghani A, Li G (2016) Smart expandable proppants to achieve sustainable hydraulic fracturing treatments. Paper SPE 181391-MS, presented in SPE annual technical conference & exhibition, Dubai, UAE
- Santos L, Dahi Taleghani A, Li G (2017) Expandable diverting agents to improve efficiency of refracturing treatments. Paper-URTeC 2697493, presented in the oral presentation at the unconventional resources technology conference in Austin, TX, USA
- Siskind RD, Smith RC (2008) Model development for shape memory polymers In: The 15th international symposium on: smart structures and materials & nondestructive evaluation and health monitoring, pp 69291H–69291H. International Society for Optics and Photonics
- Taleghani AD, Li G, Moayeri M (2016) The use of temperature-triggered polymers to seal cement voids and fractures in wells. SPE-Paper-181384-MS. Society of Petroleum Engineers
- Vickers S, Cowie M, Jones T, Allan JT (2006) A new methodology that surpasses current bridging theories to efficiently seal a varied pore throat distribution as found in natural reservoir formations. Paper AADE-06-DF-HO-16, presented at the 2006 AADE fluids conference, Houston, TX, USA, 11–12 Apr 2006
- Wang A, Li G (2015) Stress memory of a thermoset shape memory polymer. *J Appl Polym Sci* 132(24):42112
- White RJ (1956) Lost-circulation materials and their evaluation. In: *Drilling and production practice*. American Petroleum Institute
- Whitfill D (2008) Lost circulation material selection, particle size distribution and fracture modeling with fracture simulation software. SPE-115039-MS, IADC/SPE Asia Pacific drilling technology conference and exhibition, Jakarta, Indonesia, 25–27 Aug 2008

**Publisher's Note** Springer Nature remains neutral with regard to jurisdictional claims in published maps and institutional affiliations.